ACCOUNTS
of chemical research

Stability of High-Aspect-Ratio Micropillar Arrays against Adhesive and Capillary Forces

DINESH CHANDRA† AND SHU YANG*

Department of Materials Science and Engineering, University of Pennsylvania, 3231 Walnut Street, Philadelphia, Pennsylvania 19104

RECEIVED ON JANUARY 5, 2010

CONSPECTUS

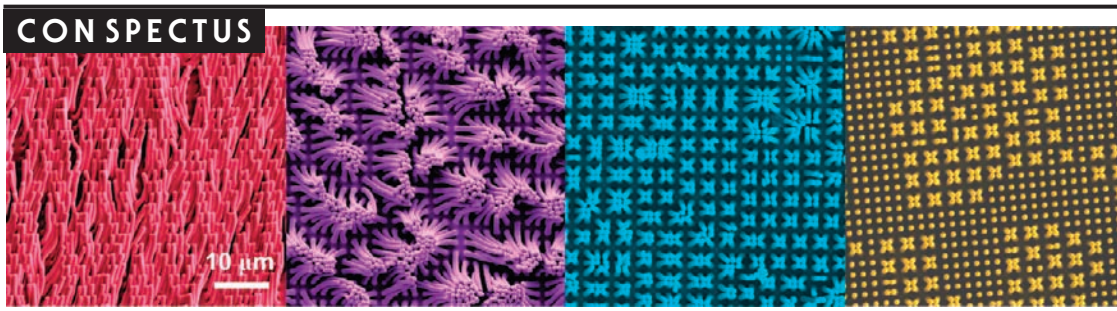

High aspect-ratio (HAR) micropillar arrays have many interesting and technologically important applications. Their properties, such as large mechanical compliance, large surface area, and a topography that is well-separated from the underlying substrate, have allowed researchers to design and explore biomimetic dry adhesives, superhydrophobic, superoleophobic, and tunable wetting surfaces, mechanical sensors and actuators, and substrates for cell mechanics studies. However, the mechanical compliance and large surface area of the micropillars also make these structures susceptible to deformation by adhesive and capillary surface forces. As a result such micropillars, particularly those made from soft polymers, can prove challenging to fabricate and to use in various applications. Systematic understanding of these forces is thus critical both to assemble stable micropillar arrays and to harness these surface forces toward controlled actuation for various applications.

In this Account, we review our recent studies on the stability of HAR polymeric micropillar arrays against adhesive and capillary forces. Using the replica molding method, we have successfully fabricated HAR epoxy micropillar arrays with aspect ratios up to 18. The stability of these arrays against adhesive forces is in agreement with theoretical predictions. We have also developed a new two-step replica molding method to fabricate HAR (up to 12) hydrogel micropillar arrays using monomers or monomer mixtures. By varying the monomer composition in the fabrication process, we have fabricated a series of hydrogel micropillar arrays whose elastic moduli in wet state range from less than a megapascal to more than a gigapascal, and we have used these micropillar arrays to study capillary force induced clustering behavior as a function of the modulus. As a result, we have shown that as liquid evaporates off the micropillar arrays, the pillars bend and cluster together because of a much smaller capillary meniscus interaction force while the micropillar structures are surrounded by a continuous liquid body. Previously, researchers had often attributed this clustering effect to a Laplace pressure difference because of isolated capillary bridges. Our theoretical analysis of stability against capillary force and micropillar cluster size as a function of pillar elastic modulus agrees well with our experimental observations.

The fabrication approaches presented here are quite general and will enable the fabrication of tall, stable micropillar arrays in a variety of soft, responsive materials. Therefore, researchers can use these materials for various applications: sensors, responsive wetting, and biological studies. The new insights into the capillary force induced clustering of micropillar arrays could improve rational design and fabrication of micropillar arrays that are stable against capillary force. In addition, these results could help researchers better manipulate capillary force to control the assembly of micropillar arrays and actuate these structures within novel devices.

Introduction

Arrays of high-aspect-ratio (HAR) microstructures (AR = ratio of height to lateral feature size, h/d, Figure 1a) present many unique features, including large surface area, a surface topography well-separated from the underlying substrate, and large

Published on the Web 06/16/2010 www.pubs.acs.org/acr
10.1021/ar100001a

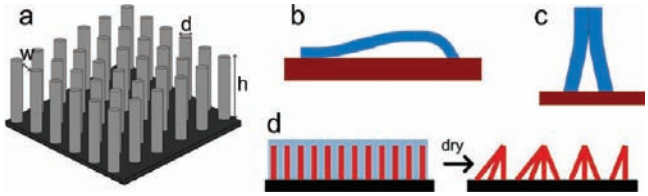

FIGURE 1. Schematics of micropillar arrays (a) and their common mechanical failure mechanisms: (b) ground collapse and (c) lateral collapse due to adhesive forces and (d) collapse due to liquid capillary force.

mechanical compliance. In Nature, these features have resulted in evolutionary functions ranging from reversible dry adhesion of gecko foot hairs[1] to the superhydrophobic surface of lotus leaves.[2] Taking advantage of their small bending stiffness at the nano- and microscale, many researchers have created arrays of HAR microstructures and investigated their potential technological applications, including reversible dry adhesives,[3] micromechanical sensors,[4] and actuators.[5] The large surface area and spatially distinct surface topography provided by tall micropillar arrays have been widely utilized for creating superhydrophobic surfaces and their dynamic tuning,[6,7] DNA separation,[8] designing efficient batteries,[9] and enhancing heat transfer.[10] However, as the dimensions of microstructures decrease and their aspect ratio increases, the surface area to volume ratio also increases significantly. Thus, the HAR microstructures become increasingly susceptible to surface forces, such as adhesive force between the microstructures[11] and liquid capillary forces when immersed and dried from a liquid,[12] leading to pattern collapse (Figure 1b–d). Recently, these forces have also been utilized to self-assemble hierarchical superstructures.[13,14] Systematic understanding of the effect of adhesive and capillary forces on the stability of HAR micropillar arrays is therefore critical to both the fabrication of high-fidelity HAR micropillar arrays and their manipulation for a wide range of applications.

HAR micropillar arrays have been fabricated by a variety of top-down and bottom-up assembly based methods, including photolithography, e-beam lithography, soft lithography, template lithography from block copolymer thin films and colloidal assembly, and templating from anodized alumina. Detailed discussion can be found in a recent review by del Campo et al.[15] These methods, however, are often limited by (a) stiff inorganic materials or materials with specific chemical functionality, (b) random defects, and (c) a certain geometry and lateral dimensions. For example, polymer microstructures with aspect ratio up to 15 have been fabricated before using soft lithography but with feature sizes typically in the range of tens to hundreds of micrometers.[16–19] In addition, many of the methods are not suitable for large-area fabrication or require multistep expensive processes. Compared with stiff inorganic materials, polymeric micropillar arrays offer many attractive properties, such as biocompatibility, tunability and responsiveness. Thus, a low-cost and high-fidelity fabrication method for polymeric micropillar arrays is highly desirable.

Using replica molding, we have fabricated HAR pillar arrays in polymeric materials, such as epoxy,[20] polyurethane,[20] and hydrogels,[13] with lateral dimensions ranging from 300 nm to 1 μm and aspect ratios up to 18 (Figures 2 and 3). By controlling the geometry and mechanical properties of these pillar arrays, we studied the stability of such structures against surface forces, such as adhesive[20] and capillary forces.[21,22] Specifically, we have re-examined the capillary force induced clustering of tall micropillars and shown that when a liquid is evaporated off the micropillar arrays, the pillars cluster together due to a much smaller capillary meniscus interaction force rather than due to the often-cited Laplace pressure difference because of isolated capillary bridges.[21] The stability analysis presented here provides insights and guidelines to fabricate and manipulate HAR micropillar arrays by tuning their geometry and mechanical and surface properties; therefore, it will open up new avenues of applications of tall polymer pillar arrays and their clusters.

In the following sections, we present some of our recent results on fabrication of polymeric micropillar arrays, study of their stability against adhesive and capillary forces, and an exemplary application of HAR hydrogel pillar clusters as ultrathin whitening layers. Finally, we conclude with a future outlook.

Fabrication of Polymeric Micropillar Arrays

Fabrication of Epoxy Micropillar Arrays.[20] The epoxy micropillars, including cone-shape, circular, and square cylinders, were replicated from the corresponding Si masters through poly(dimethylsiloxane) (PDMS) negative molds. The width (or diameter), d, of the Si pillars ranged from 300 nm to 1 μm, the height h ranged from 7 to 9 μm, and the spacing w between pillars ranged from 400 nm to 1.32 μm.

In the molding process, liquid precursors infiltrate into the mold channels by capillary action, and the complete filling time t can be estimated as

$$t = \frac{2\eta_m h^2}{R\gamma_m \cos\theta} \quad (1)$$

where η_m is the viscosity of the molding liquid precursor, R is the hydraulic radius of the pores, γ_m is the surface tension of the molding liquid precursor, and θ is the contact angle between the molding liquid and the surface of the mold chan-

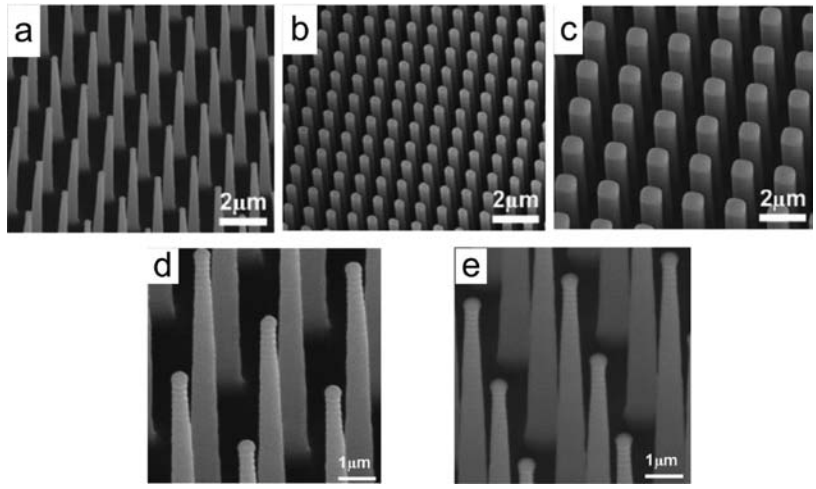

FIGURE 2. Scanning electron microscopy (SEM) images of epoxy micropillar arrays fabricated by replica molding method: (a) conical micropillars, $h = 7$ μm, d (tip) = 300 nm, d (bottom) = 680 nm, $w = 1.32$ μm (at base); (b) circular cross-section micropillars, $h = 9$ μm, $d = w = 500$ nm; (c) square cross-section micropillars, $h = 9$ μm, $d = w = 1$ μm; (d, e) fine features on the conical micropillar arrays (d) as replicated from the features on the original silicon micropillar arrays (e).

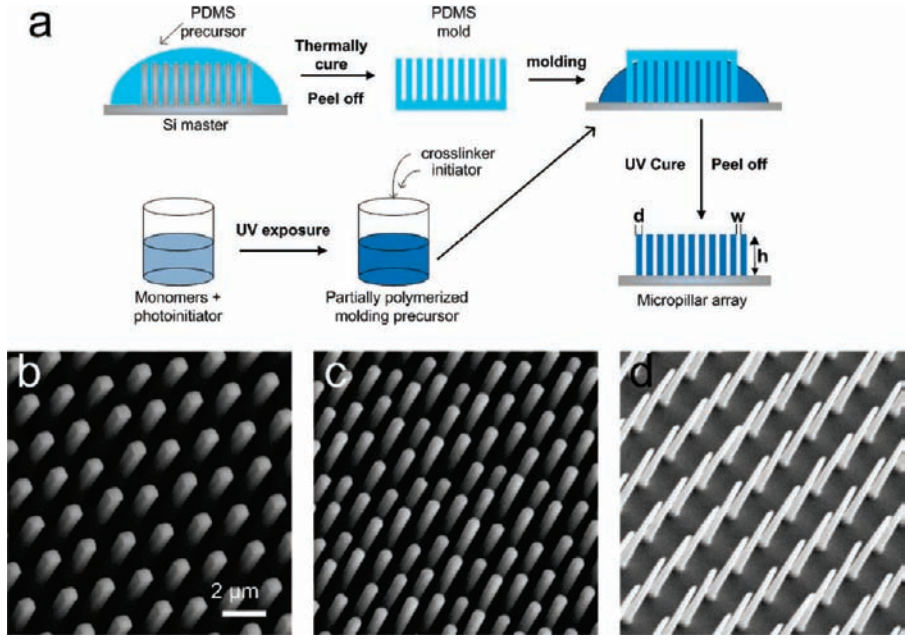

FIGURE 3. (a) Schematic illustration of the fabrication of hydrogel micropillar arrays by the modified replica molding process. (b–d) SEM images of PHEMA hydrogel pillar arrays in three different geometries: (b) pillars with square cross-section, $h = 9$ μm, $d = w = 1$ μm; (c) pillars with circular cross-section, $h = 9$ μm, $d = w = 750$ nm; (d) conical micropillars, $h = 7$ μm, d (tip) = 350 nm, d (bottom) = 750 nm, $w = 1.25$ μm (at base). Scale bar in panel b applies to all the SEM images.

nel. Lower contact angle (i.e., higher wettability) of molding liquid on PDMS mold is preferred for complete filling at a shorter period of time. For the deepest pores ($h = 9$ μm), the required complete filling time of epoxy is estimated as ~0.1 s. Typically, the epoxy liquid was left on the PDMS mold for ≥2 min.

Because of the elastomeric nature and low surface energy of PDMS, the mold could be easily separated from the cured micropillars without damaging either the replicated structure or the mold. The porous nature of the PDMS and high surface area to volume ratio of the HAR channels in the mold allows easy diffusion of air within the channels while molding, resulting in bubble-free replication of the micropillars in various geometries with aspect ratio up to 18 (Figure 2a–c). A comparison of the fine structures present in the original Si micropillars to those in the epoxy replica (Figure 2d,e) further demonstrates the high fidelity of the molding process.

Fabrication of Hydrogel Micropillar Arrays.[13,22] Because of their biocompatibility, softness, and porous nature, hydrogels are of interest in living cell studies and tissue engineering. Their chemical nature can be easily tailored, and

TABLE 1. Comparison of Theoretical and Experimental Stability of Epoxy ($E \approx 3$ GPa) and Polyurethane ($E \approx 138$ MPa) Micropillar Arrays against Lateral Collapse Due to Adhesive Forces

	pillar array geometry			epoxy		polyurethane	
pillar cross-section	d (nm)	w (nm)	aspect-ratio	critical aspect ratio and predicted stability	observed stability	critical aspect ratio and predicted stability	observed stability
circular	750	750	12	21.3 (stable)	stable	8.1 (unstable)	stable
circular	500	500	18	18.6 (stable)	stable	7 (unstable)	unstable
circular	400	400	22.5	17.3 (unstable)	unstable	6.5 (unstable)	unstable
circular	400	650	22.5	22 (unstable)	unstable	8.4 (unstable)	unstable
square	1000	1000	9	12.4 (stable)	stable	6 (unstable)	stable

many of them are sensitive to external stimuli, such as pH, temperature, and electric field making them attractive for applications in sensors and actuators. We fabricated various poly(2-hydroxylethyl methacrylate) (PHEMA)-based hydrogel micropillar arrays,[13,22] where the mechanical property and chemistry of the final structures can be tuned by altering the starting monomer compositions. However, directly molding hydrogels from their monomers using PDMS molds was found to be problematic. Not only did the monomers easily diffuse into the molds, but the oxygen dissolved in the mold could diffuse in the molding material and inhibit the free-radical polymerization and cross-linking of the gels within the PDMS channels. These problems become even more critical in the case of HAR pillar arrays, where their large surface area to volume ratio enhances the diffusion of oxygen and monomers. To prevent this problem, we modified the molding process and fabricated the hydrogel HAR pillar arrays in two steps (Figure 3a).[13] First, the monomers were mixed with photoinitiator and partially polymerized under UV light to obtain a viscous molding precursor. In the second step, this precursor was molded and UV-cured after adding cross-linker and additional photoinitiator. The increased viscosity of precursor liquid effectively prevents both the monomer diffusion in the mold and the oxygen diffusion in the molding precursor. Using this method, we have fabricated hydrogel micropillar arrays in three different geometries with aspect ratios up to 12 (Figure 3b−d) from a variety of monomers, including 2-hydroxyethyl methacrylate[13,22] (HEMA), *N*-isopropylacrylamide[13] (NIPA), ethylene glycol dimethacrylate (EGDMA),[13] and methyl methacrylate (MMA).[22]

Stability of Micropillar Arrays against Adhesive Force

As seen from Figures 2 and 3, the fabricated epoxy and hydrogel HAR micropillar arrays are stable in air, which can be attributed to the high elastic modulus of the pillars (see also Tables 1 and 2). For example, the modulus of cured epoxy and hydrogels is ~3 GPa and >1.5 GPa, respectively. We also fabricated pillars in materials with lower elastic modulus, such as polyurethane (~138 MPa) and PDMS (~1.7 MPa)[20] to better understand the stability of micropillar arrays. Hui et al. have suggested that soft, HAR microstructures, such as from PDMS, can buckle under their own weight.[23] The critical height of the microstructures, h_c, above which they are unstable against the gravity induced buckling, is given as

TABLE 2. Comparison between Measured Elastic Modulus and Critical Modulus for Stability against Lateral Collapse for the Stable Hydrogel Micropillar Arrays

	surface energy, γ_s (mN/m)	critical modulus for collapse, E_c, (MPa)			Young's modulus, E (MPa)
		square cross-section	circular cross-section	conical micropillars	
PHEMA	33.4 ± 0.1	584	380	83	1790 ± 12
PHEMA-*co*-PNIPA	32.7 ± 0.3	572	373	82	1825 ± 8
PEGDMA	37.6 ± 0.2	658	429	94	1582 ± 26

$$h_c = \left(\frac{0.49Ed^2}{\rho g}\right)^{1/3} \quad (2)$$

where d is the diameter of the micropillar, E and ρ are the elastic modulus and density of the micropillar material, respectively, and g is the gravitational acceleration. However, as Roca-Cusachs and co-workers pointed out,[24] according to the gravitational model of collapse (eq 2) the critical aspect ratio for stability, $(h/d)_c$, scales as $d^{-1/3}$, suggesting that as the diameter decreases, the pillars should be more stable at higher aspect ratios. In particular, as the diameter tends to zero, the stable aspect ratio tends to infinity, which is clearly not true. Instead, Roca-Cusachs et al. suggested that at smaller dimensions, (sub)micrometer regime, adhesion between the pillar and the substrate and between the pillars themselves dominates over gravity and becomes the main cause for ground collapse (Figure 1b) or lateral collapse (Figure 1c) of the micropillars. By balancing the bending energy of the ground collapsed micropillar with the energy of pillar adhesion to the substrate, Roca-Cusachs et al.[24] derived the expression for the critical aspect ratio, $(h/d)_c$, for ground collapse, below which the micropillars are stable,

$$\left(\frac{h}{d}\right)_c = \frac{\pi^{5/3}}{2^{11/3}3^{1/2}}(1-\upsilon^2)^{-1/6}\left(\frac{E}{2\gamma_{sv}}\right)^{2/3}d^{2/3} \quad (3)$$

where υ is the Poisson's ratio for the pillar material and γ_{sv} is the surface energy of the pillar material.

Additionally, the micropillars can bend laterally and adhere to the neighboring pillars. The lateral collapse is more dominant in high density arrays, where due to small interpillar distances, only a small amount of bending is required for the pillars to adhere together. By balancing the bending energy and the energy of deformation (to make adhesion over a finite area) of laterally adhered pillars with their energy of adhesion, Glassmaker et al.[11] derived expressions for the critical aspect ratio against lateral collapse for pillars with circular cross-section,

$$\left(\frac{h}{d}\right)_c = \left(\frac{3^{3/4}\pi E w^{3/2}}{2^{1/4}32\gamma_{sv}(1-\upsilon^2)^{1/4}d^{1/2}}\right)^{1/3} \quad (4)$$

and for pillars with square cross-section,

$$\left(\frac{h}{d}\right)_c = \left(\frac{3Ew^2}{8d\gamma_{sv}}\right)^{1/4} \quad (5)$$

where w is the lateral separation between adjacent micropillars (see Figure 1). For a given micropillar array geometry, the above equations can be rearranged to obtain a critical elastic modulus, E_c (E_c^l for lateral collapse and E_c^g for ground collapse), below which the micropillars are unstable.

For the pillars with the smallest diameter and the highest aspect ratio (d = 400 nm and AR = 22.5), E_c^g estimated by eq 3 is ~117 MPa, smaller than the moduli of epoxy, polyurethane, and the hydrogel systems. In agreement with the theory, experimentally all the epoxy, polyurethane, and the hydrogel micropillar arrays were stable against ground collapse whereas PDMS pillars, which had a much lower modulus, ~1.7 MPa, did collapse to ground due to adhesive force (Figure 4a). The epoxy and polyurethane pillar arrays could collapse laterally depending on their geometries (Figure 4b). Tables 1 and 2 summarize our comparison between the theoretically predicted (from eqs 4 and 5) and experimentally observed stability against lateral collapse in different systems of polymer pillar arrays. Good agreement between the experimental observation and theoretical prediction shows that the balance between adhesive and elastic forces can be controlled by manipulating the geometry and elastic modulus of the pillar arrays. For a given aspect ratio and material, stability can be increased by either increasing the interpillar spacing or decreasing the surface energy of the pillars. We demonstrated the latter point by partially restoring the collapsed micropillars[20] through treating them with low surface energy supercritical CO_2.

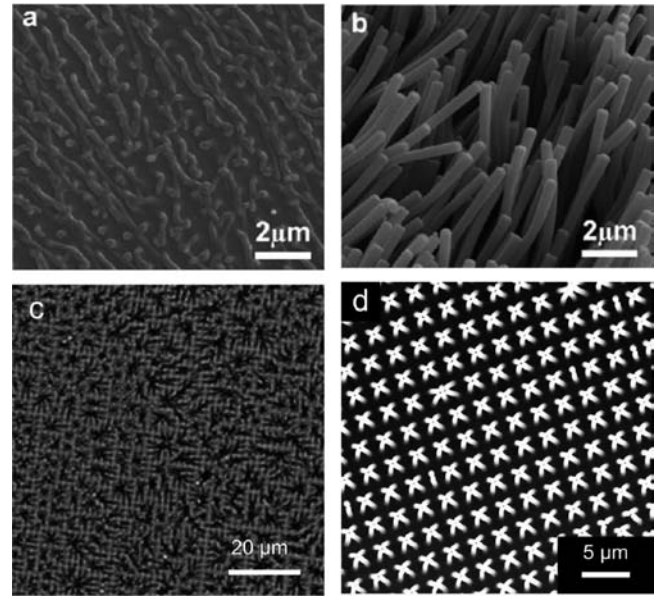

FIGURE 4. Failure mechanisms observed in various fabricated polymer pillar arrays: (a) PDMS nanopillar array (h = 9 μm, $d = w$ = 500 nm) ground collapsed due to adhesive forces; (b) polyurethane nanopillar array (h = 9 μm, $d = w$ = 500 nm) collapsed laterally due to adhesive forces; (c) PEGDMA micropillar array (h = 7 μm, d (tip) = 350 nm, d (bottom) = 750 nm, w (at base) = 1.25 μm) collapsed due to ethanol capillary force; (d) PEGDMA micropillar array (h = 9 μm, $d = w$ = 750 nm) clustered in a regular pattern due to ethanol capillary force.

Stability of Micropillar Arrays against Capillary Force

In many applications, such as biological studies and microfluidics, and fabrication processes, such as photolithography, the pillar arrays are exposed to liquid and can collapse due to capillary force when the liquid evaporates off their surface. For example, when ethanol was evaporated off the PEGDMA pillar arrays, the pillars clustered together (Figure 4c,d). On the other hand, capillary force can be utilized to assemble periodic superstructures as demonstrated by us[13] (Figure 4d) and others.[14] In this section, we focus on the capillary force induced clustering of micropillar arrays.

Capillary Force in 2D Arrays of Micropillars. In general, the capillary force is proportional to the liquid−vapor interfacial energy γ and results from the tendency of a system to minimize the sum of the three interfacial energies, liquid−vapor (γ), solid−vapor (γ_{sv}), and solid−liquid (γ_{sl}), which are related to each other through the Young's equation, $\gamma_{sv} - \gamma_{sl} - \gamma\cos\theta = 0$, where θ is the equilibrium contact angle. The exact expression for the capillary force, however, depends on the geometry of the system and gives rise to a range of phenomena, such as collapse of photoresist patterns due to negative Laplace pressure of capillary bridges,[25] buckling of microfilaments due to liquid surface tension,[26] coalescence of

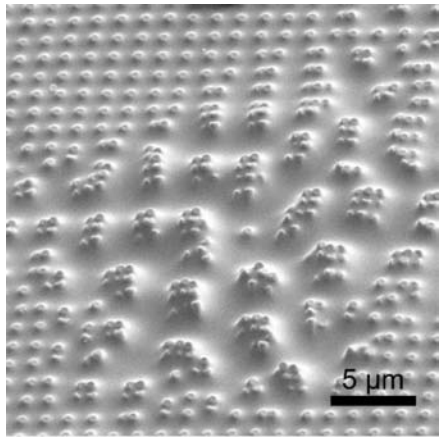

FIGURE 5. SEM image of epoxy pillar arrays ($d = 0.6$ μm, $h = 4.8$ μm, $w = 0.9$ μm) collapsed by polystyrene melt.

fibers driven by reduction in liquid−vapor surface area,[27,28] and aggregation of particles partially immersed in or floating on a liquid surface due to lateral forces arising from capillary menisci interaction.[29] All of these phenomena, though equivalent in terms of the driving force arising from minimization of total surface energy, are very different in terms of geometry and magnitude of the forces.

In the literature, distortion of one-dimensional (1D) arrays of tall line patterns, when a liquid is evaporated off the surface, has been explained by Laplace pressure difference due to isolated capillary bridges formed between the structures.[25] The same argument is often extended to explain the instability of two-dimensional (2D) arrays of micropillars.[30−32] Occasionally, the collapsing behavior of 2D micropillar arrays has been attributed to lateral forces arising from interaction between capillary menisci formed around the microstructures,[33] and often no distinction is made between these two approaches.

In our recent work,[21] we showed experimentally that in the case of 2D arrays of micropillars, when a liquid is evaporated off their surface, the clustering should be attributed to the lateral forces resulting from capillary menisci interaction rather than to Laplace pressure difference due to isolated capillary bridges. Our calculation indicates that the capillary meniscus interaction force can be more than an order of magnitude smaller than that obtained by assuming Laplace pressure difference due to capillary bridges. Consequently, the critical elastic modulus necessary for the stability of the micropillars is much smaller.

We used short chain polystyrene (PS) melt ($M_n = 1.79$ kg/mol and PDI = 1.06) as the wetting liquid on epoxy pillar arrays (2D square lattice, $d = 0.6$ μm, $h = 4.8$ μm, $w = 0.9$ μm) to study capillary-induced collapsing behavior and to directly visualize the liquid morphology between the pillars. The key observation (Figure 5) was that when the liquid PS is evaporated off the micropillar arrays, the pillars collapse while still completely surrounded by PS liquid except at the tips. The absence of isolated capillary bridges between the pillars and the fact that a continuous liquid body in equilibrium has a spatially constant Laplace pressure[34] indicate that Laplace pressure difference cannot explain the observed collapse of pillars. Atomic force microscopy (AFM) imaging of PS frozen in a mechanically stable, low-aspect-ratio micropillar array further confirmed that the mean curvature, and thus the Laplace pressure in the liquid surrounding the micropillars, is constant everywhere. It should be noted that for 1D line patterns, the Laplace pressure argument is valid because isolated liquid between the lines could exist, resulting in different Laplace pressures.

Indeed, even in absence of Laplace pressure variation, two particles partially immersed in a liquid or floating on a liquid interface experience a lateral capillary meniscus interaction force[35] (Figure 6a), which can be either attractive (when the particles are both hydrophobic or both hydrophilic) or repulsive (when the particles have opposite wettabilities). This lateral force arises because of the deformation of the otherwise flat liquid surface due to presence of the particles. When two particles of same wettability come closer, the overall deformation of the liquid surface decreases due to overlap, giving rise to attractive potential between the particles. The collapsing mechanism of micropillars due to these lateral forces is illustrated in Figure 6c. Based on the equations given by Kralchevsky et al.,[36] we derived an expression for the capillary force between two cylinders partially immersed in a liquid as

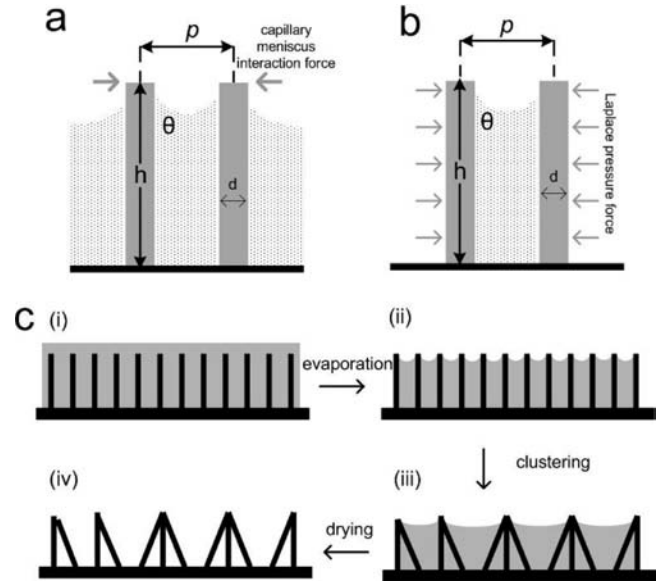

FIGURE 6. Schematic illustrations of forces acting on two pillars, (a) partially immersed in a liquid and (b) with an isolated capillary bridge between them. (c) Mechanism of clustering in micropillar arrays induced by lateral capillary meniscus interaction force.

$$F_C = -\frac{\partial W_c}{\partial p} = -\frac{\pi\gamma d^2 \cos^2\theta}{2\sqrt{p^2 - d^2}} \quad (6)$$

where W_c is the capillary interaction energy of two cylinders, d is the diameter of the cylinders, and p is the center-to-center distance between them (Figure 6a). In the case of micropillars, where one end is fixed on the substrate, the bending torque τ_c on the pillars due to the lateral capillary force is

$$\tau_c = \frac{\pi\gamma d^2 h \cos^2\theta}{2\sqrt{p^2 - d^2}} \quad (7)$$

In the case of an isolated capillary bridge between the pillars (Figure 6b), the Laplace pressure difference is approximately $P_l \approx (2\gamma \cos\theta)/(p - d)$, and thus the torque on the pillars is

$$\tau_l \approx \frac{\gamma d h^2 \cos\theta}{p - d} \quad (8)$$

The ratio of two types of torques is

$$\frac{\tau_l}{\tau_c} \approx \frac{2h}{\pi d \cos\theta}\sqrt{\frac{p + d}{p - d}} \quad (9)$$

For a typical case of $\theta = 60°$ and aspect ratio of 10, the torque due to the isolated capillary bridge is at least 12 times greater than that from lateral capillary meniscus interaction. The large difference in the torques is reflected in a large variation in the estimated critical modulus for stable micropillar arrays. It has been observed by us and others that in a square lattice of micropillar array, the collapsing due to evaporation of a liquid is initiated by groups of four neighboring pillars clustering together.[13,14,32] Thus, in a simple model, we considered four pillars partially immersed in a liquid on the corners of a square (Figure 7a, inset). By equating the capillary force, F_C, to the elastic restoring force, F_E, of the bent pillars as a function of pillar deflection, δ (Figure 7a), we obtained an expression of critical modulus for stability of the micropillars:[21]

$$E_{crit} = \frac{32\sqrt{2}\gamma \cos^2\theta h^3}{3d^4} f(r) \quad (10)$$

where $f(r)$ is a function of $r = p/d$ (see Figure 7b).

In comparison, for the same geometry, E'_{crit} based on Laplace pressure difference due to isolated capillary bridge between the four pillars is given by,[13,37]

$$E'_{crit} = [128\gamma h^3(3h \cos\theta + w' \sin\theta + \sqrt{9h^2 \cos^2\theta + 3hw' \sin(2\theta)})]/[3\pi d^3 (w')^2] \quad (11)$$

Here, $w' = \sqrt{2}p - d$ is the spacing between the diagonally opposite micropillars. As an example, for epoxy micropillar arrays of $h = 9\ \mu$m, $d = 0.75\ \mu$m, $p = 1.5\ \mu$m, and a contact angle $\theta = 60°$, E_{crit} is calculated as 2 GPa from eq 10, which is considerably smaller than E'_{crit} calculated as 27 GPa from eq 11.

It must be pointed out though, that in later stages of liquid evaporation, there may no longer be a continuous liquid body surrounding the micropillars and isolated capillary bridges may likely form. However, such bridges will be near the base of the micropillars, and thus will exert much less torque compared with a capillary bridge spanning the whole micropillar length.

Capillary Force Induced Clustering Behavior of Micropillar Arrays. To test the above arguments, we prepared a series of micropillar arrays in two different geometries, A ($d = 0.75\ \mu$m, $h = 9\ \mu$m, and $p = 1.5\ \mu$m) and B ($d = 1\ \mu$m, $h = 9\ \mu$m, $p = 2\ \mu$m), from copolymers of PHEMA and poly(methyl methacrylate)

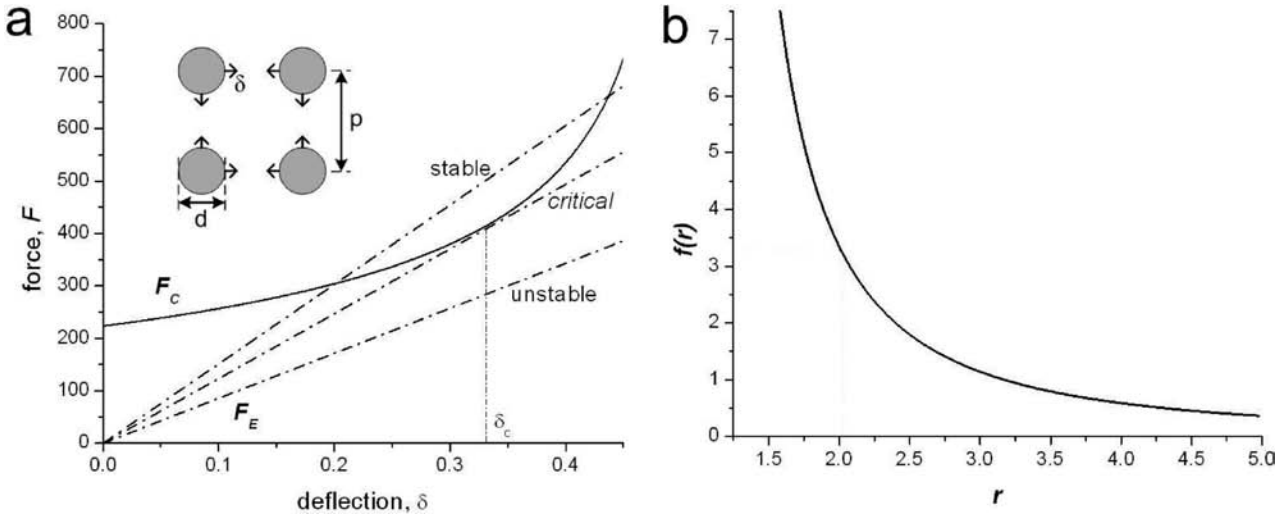

FIGURE 7. (a) A typical plot of capillary interaction force, F_C (solid line), and elastic restoring force acting on the deflected pillar, F_E (dashed lines). Increasing slope of F_E corresponds to increasing elastic modulus E. Inset shows a schematic illustration of interaction between a group of four pillars on a square lattice. (b) $f(r)$ as a function of $r = p/d$.

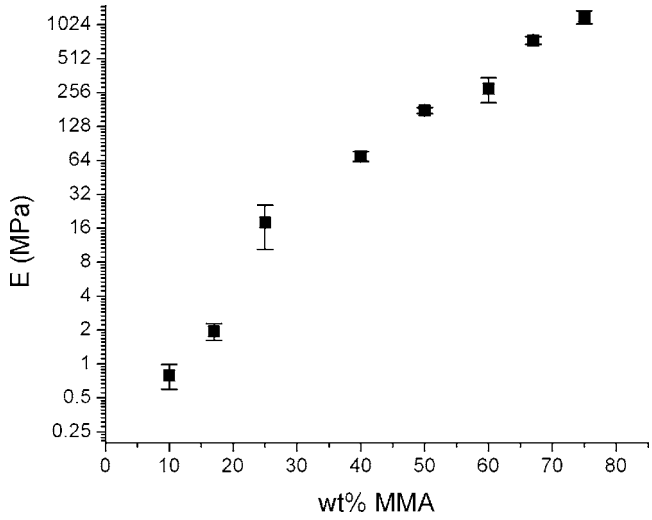

FIGURE 8. Elastic modulus in the wet state of flat PHEMA-*co*-PMMA films as a function of MMA content.

(PMMA) and studied their capillary-induced clustering.[22] The micropillar arrays were soaked in water and dried in a stream of air to induce clustering (Figure 6c). Because PMMA is glassy and does not absorb water, whereas PHEMA does, we tuned the modulus of the micropillars in the wet state over 3 orders of magnitude (~0.5 MPa to ~1.2 GPa) simply by varying the ratio of HEMA and MMA in the molding precursors (Figure 8). As seen from Figures 8 and 9, the cluster size decreases with increasing modulus and decreasing aspect ratio.

We analyzed the clustering behavior in terms of competition between capillary meniscus interaction energy and the elastic bending energy of the pillars.[22] As the pillars bend to form a cluster, the interpillar distances at the tip decrease (Figure 10a), resulting in a decrease in the capillary energy according to eq 6 and an increase in the elastic bending energy. In a cluster, since the outer pillars (higher n in Figure 10a) have to bend more than the inner ones (lower n), the bending energy per pillar increases with increasing cluster size whereas the decrease in capillary energy per pillar remains the same, resulting in a minimum cluster energy for a critical cluster size, N_c, given by

$$E = \frac{64\gamma \cos^2\theta h^3}{d^2 w^2} \times \left(\frac{(4n_c - 1)\ln(\sqrt{3}+2) + (4n_c - 2)\ln\left(\frac{\sqrt{7}+2\sqrt{2}}{\sqrt{2}+1}\right)}{8{n_c}^3 - n_c} \right) \quad (12)$$

where the number of pillars in a cluster $N_c = 4{n_c}^2$. Approximately solving eq 12 in terms of N_c reveals a linear relation between N_c and $1/E$ as

$$N_c \approx \frac{273 \cos^2\theta \gamma h^3}{E d^2 w^2} \quad (13)$$

We plotted experimentally observed values of N_c versus $1/E$ for both pillar array geometries A and B in Figure

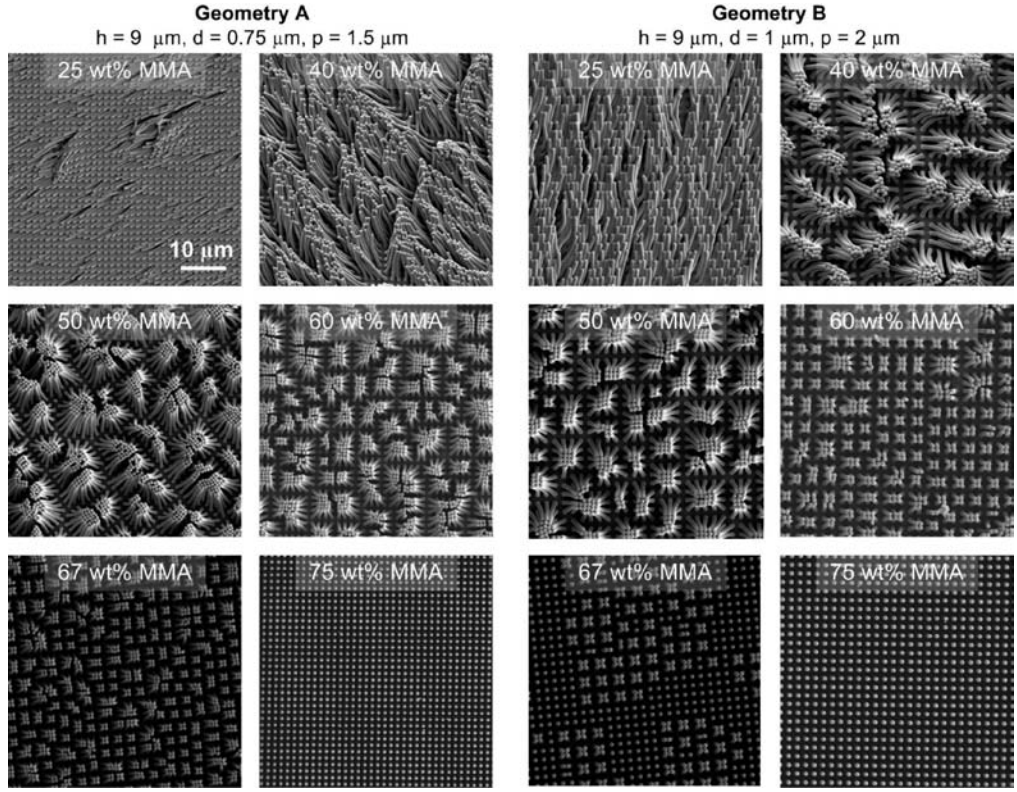

FIGURE 9. SEM images of PHEMA-*co*-PMMA micropillar arrays clustered by water capillary force.

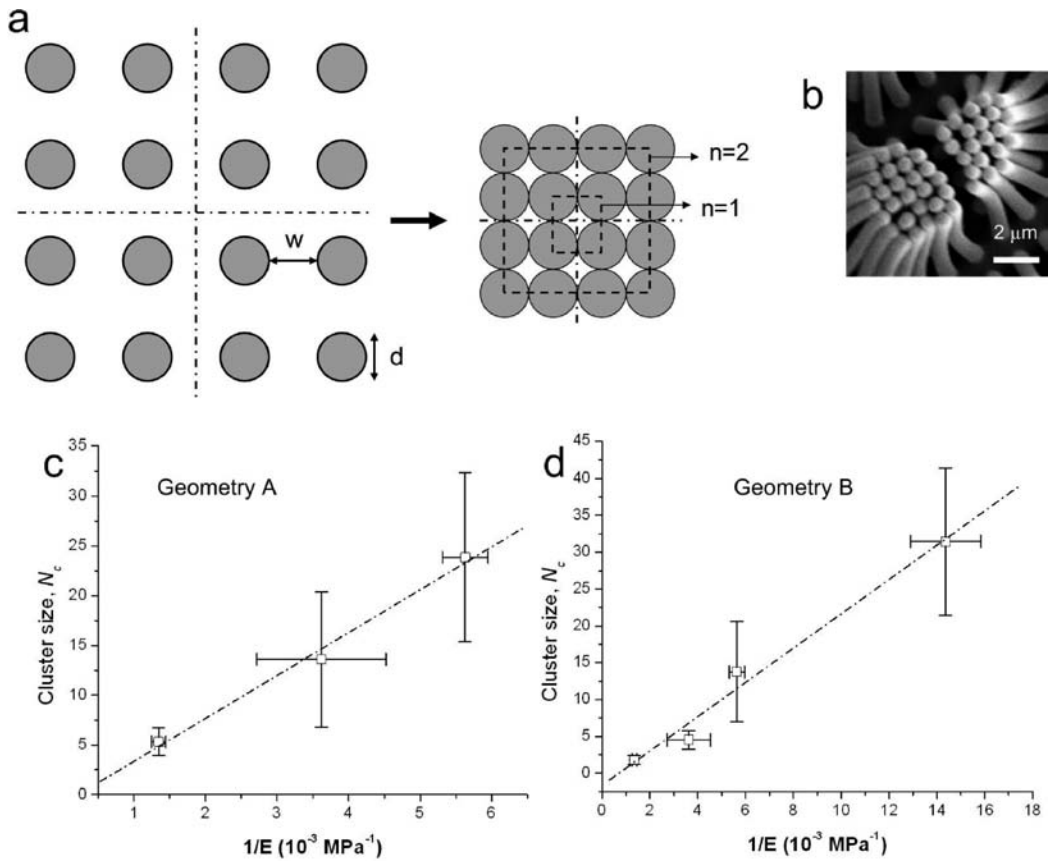

FIGURE 10. (a) Schematic illustration of micropillar array clustering in a square lattice. (b) SEM image of micropillars clustered in a square lattice. (c,d) Micropillar cluster size as a function of the elastic modulus of PHEMA-*co*-PMMA micropillars in wet state for geometry A (c) and geometry B (d). See description of two geometries in Figure 9. Dashed lines are linear fit ($r^2 = 0.99$ and 0.98 in panels c and d, respectively) to experimental data.

10c,d. The linear fit to the experimental data by eq 13 yields contact angle (θ) values of 72° for geometry A and 66° for geometry B, which were close to the measured 73°. A different scaling of cluster size N_c with the modulus E, $N_c \approx E^{-2/3}$, has also been suggested,[28,38] which results from minimization of total energy of all clusters instead of a single cluster. However, it requires intercluster interaction and rearrangement to reach the minimum energy state for the whole system, which is not possible in our system with relatively low AR (9 for geometry B and 12 for geometry A, respectively).[39]

Further, E_{crit} by eq 10 (based on capillary meniscus interaction force) is estimated as 714 and 226 MPa for geometries A and B, respectively ($\theta = 73°$), close to the experimentally suggested range (see Figures 8 and 9). In comparison, E'_{crit} by eq 11 (based on Laplace pressure due to isolated capillary bridge) is estimated as 16.7 GPa (geometry A) and 4.1 GPa (geometry B), much larger than 1.2 GPa, for which the micropillars in both geometries were found stable experimentally (Figures 8 and 9).

Finally, as a proof of concept, we demonstrated the utility of clustered micropillar arrays as ultrathin whitening layers. In traditional systems such as papers and textiles, the whitening film thickness exceeds 100 μm, and whiteness is often enhanced by pigmentation or by fluorescent dyes. Nature, however, provides elegant examples of structural whiteness such as shown in the scales of white beetles, where their color results from light scattering from a random network of microfilaments that is only a few micrometers thick.[40] Before collapsing, our micropillar arrays had a colorful appearance due to Bragg diffraction of light (Figure 11a, left). After formation of random clusters, however, the film appeared white due to random light scattering, like the scales of the white beetle (Figure 11a, right). We characterized the whiteness of the clustered arrays by measuring the CIE lightness index, L (a scale of 0 to 100, 0 being

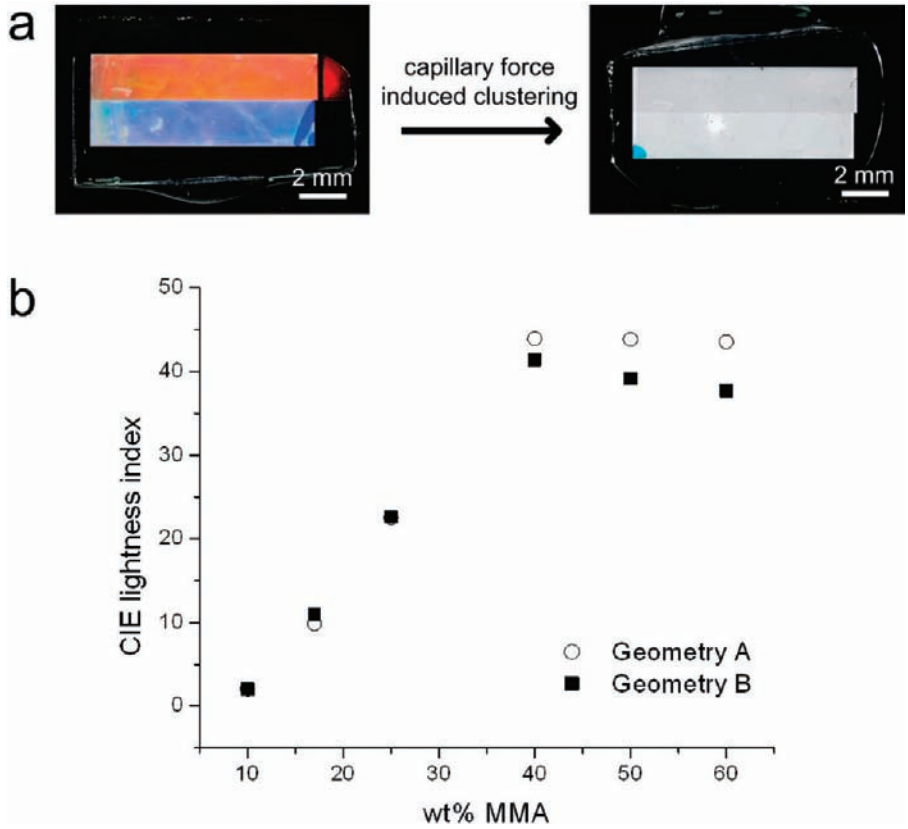

FIGURE 11. Whiteness caused by randomly clustered PHEMA-*co*-PMMA micropillar arrays shown in Figure 9. (a) Optical images of micropillar arrays before and after clustering. Two different colors in panel a (left) result from Bragg diffraction from micropillar arrays with two different periodicities. (b) CIE lightness index of the clustered micropillar arrays at different MMA contents.

black and 100 being perfect white) (Figure 11b). The whiteness increased as the randomly clustered structure evolved with increasing elastic modulus of the pillars, and we could achieve a maximum L value of ~45 for our structures, which were less than 9 μm thick (the micropillar height). In comparison, conventional uncoated paper has lightness index of ~70 and is over 120 μm in thickness.[40]

The theoretical and experimental investigation presented above regarding the critical elastic modulus and the cluster size convincingly confirm that in 2D arrays of tall micropillars, capillary meniscus interaction, rather than the Laplace pressure difference due to isolated capillary bridges, is the reason for clustering upon liquid drying. The above analysis can be utilized to achieve capillary-based controlled assembly and actuation of pillar arrays. For example, ordered assembly as shown in Figure 4d can be achieved in square lattice and other geometries by designing pillar arrays close to their critical modulus for stability (eq 10). Further, the pillars can be actuated from clustered to unclustered states by using responsive materials for pillars and dynamically varying the environmental stimulus for actuation.[5,14]

Conclusion and Future Perspective

In this Account, we have reviewed our recent progress in studying the stability of tall polymeric micropillar arrays against adhesive and capillary forces. We have fabricated stable HAR pillar arrays in a variety of polymers and introduced a new approach to fabricate hydrogel micropillar arrays, when the polymerization is sensitive to environmental oxygen. We have identified control parameters for maintaining the pillar stability, as well as their clustering. Increasing interpillar separation and low surface energy favors stability against adhesive forces. Designing micropillar arrays close to their critical stability modulus against capillary force promotes capillary-induced regular assembly of micropillars. In addition, we have suggested capillary-induced actuation of micropillars by dynamically changing the surface energies. Finally, in the context of capillary force, we have shown that contrary to the often-reported isolated capillary bridges, micropillars collapse

due to a much smaller capillary meniscus interaction force, resulting in important implications for the stability of the micropillars.

The detailed experiments regarding adhesive forces in micropillar arrays and new insights into the capillary force induced clustering of micropillar arrays will offer important guidelines for rational design and fabrication of stable micropillar arrays in dry and liquid environments and pave new ways toward capillary manipulation of micropillars for applications in areas of sensors, responsive surfaces, and biological studies.

This work is in part supported by the National Science Foundation (BES-0438004, CAREER/DMR-0548070, and MRSEC/DMR-0520020). We acknowledge the Penn Regional Nanotechnology Facility for access to AFM and SEM.

BIOGRAPHICAL INFORMATION

Dinesh Chandra completed his undergraduate studies in Metallurgical Engineering and Materials Science at the Indian Institute of Technology, Bombay, and received his B. Tech. and M. Tech. degrees in 2004. He pursued his doctoral studies with Prof. Shu Yang at University of Pennsylvania in the Department of Materials Science and Engineering and received his M.S. degree in 2006 and Ph.D. degree in 2009. Currently, he is a Postdoctoral Research Associate with Prof. Alfred J. Crosby in the Polymer Science and Engineering Department at University of Massachusetts, Amherst. His research interests include capillary force at the microscale and surface mechanical instabilities in polymers.

Shu Yang is an Associate Professor in the Department of Materials Science and Engineering at the University of Pennsylvania. She received her B.S. degree in Materials Chemistry from Fudan University, China, in 1992 and Ph.D. degree in Chemistry and Chemical Biology under the supervision of Professor Christopher K. Ober in the Department of Materials Science and Engineering at Cornell University in 1999. She then joined Bell Laboratories, Lucent Technologies, as a Member of Technical Staff before moving to Penn in 2004. Her current research includes synthesis and engineering of well-defined polymers and inorganic materials with controlled size, shape, and morphology over multiple length scales and study of their directed assembly and unique surface, optical, and mechanical properties.

FOOTNOTES

*E-mail: shuyang@seas.upenn.edu.

†Current Address: Department of Polymer Science and Engineering, University of Massachusetts, Amherst, 120 Governors Drive, Amherst, Massachusetts 01003.

REFERENCES

1 Autumn, K.; Liang, Y. A.; Hsieh, S. T.; Zesch, W.; Chan, W. P.; Kenny, T. W.; Fearing, R.; Full, R. J. Adhesive force of a single gecko foot-hair. *Nature* **2000**, *405*, 681–685.

2 Barthlott, W.; Neinhuis, C. Purity of the sacred lotus, or escape from contamination in biological surfaces. *Planta* **1997**, *202*, 1–8.

3 Northen, M. T.; Greiner, C.; Arzt, E.; Turner, K. L. A gecko-inspired reversible adhesive. *Adv. Mater.* **2008**, *20*, 3905–3909.

4 du Roure, O.; Saez, A.; Buguin, A.; Austin, R. H.; Chavrier, P.; Siberzan, P.; Ladoux, B. Force mapping in epithelial cell migration. *Proc. Natl. Acad. Sci. U.S.A.* **2005**, *102*, 2390–2395.

5 Evans, B. A.; Shields, A. R.; Carroll, R. L.; Washburn, S.; Falvo, M. R.; Superfine, R. Magnetically actuated nanorod arrays as biomimetic cilia. *Nano Lett.* **2007**, *7*, 1428–1434.

6 Li, X. M.; Reinhoudt, D.; Crego-Calama, M. What do we need for a superhydrophobic surface? A review on the recent progress in the preparation of superhydrophobic surfaces. *Chem. Soc. Rev.* **2007**, *36*, 1350–1368.

7 Krupenkin, T. N.; Taylor, J. A.; Schneider, T. M.; Yang, S. From rolling ball to complete wetting: The dynamic tuning of liquids on nanostructured surfaces. *Langmuir* **2004**, *20*, 3824–3827.

8 Kaji, N.; Tezuka, Y.; Takamura, Y.; Ueda, M.; Nishimoto, T.; Nakanishi, H.; Horiike, Y.; Baba, Y. Separation of long DNA molecules by quartz nanopillar chips under a direct current electric field. *Anal. Chem.* **2004**, *76*, 15–22.

9 Kim, M. G.; Cho, J. Reversible and high-capacity nanostructured electrode materials for Li-ion batteries. *Adv. Funct. Mater.* **2009**, *19*, 1497–1514.

10 Chen, R.; Lu, M. C.; Srinivasan, V.; Wang, Z.; Cho, H. H.; Majumdar, A. Nanowires for enhanced boiling heat transfer. *Nano Lett.* **2009**, *9*, 548–553.

11 Glassmaker, N. J.; Jagota, A.; Hui, C.-Y.; Kim, J. Design of biomimetic fibrillar interfaces: 1. Making contact. *J. R. Soc. Interface* **2004**, *1*, 23–33.

12 Kotera, M.; Ochiai, N. Three-dimensional simulation of resist pattern deformation by surface tension at the drying process. *Microelectron. Eng.* **2005**, *78–79*, 515–520.

13 Chandra, D.; Taylor, J. A.; Yang, S. Replica molding of high-aspect-ratio (sub-)micron hydrogel pillar arrays and their stability in air and solvents. *Soft Matter* **2008**, *4*, 979–984.

14 Pokroy, B.; Kang, S. H.; Mahadevan, L.; Aizenberg, J. Self-organization of a mesoscale bristle into ordered, hierarchical helical assemblies. *Science* **2009**, *323*, 237–240.

15 del Campo, A.; Arzt, E. Fabrication approaches for generating complex micro- and nanopatterns on polymeric surfaces. *Chem. Rev.* **2008**, *108*, 911–945.

16 Marques, C.; Desta, Y. M.; Rogers, J.; Murphy, M. C.; Kelly, K. Fabrication of high-aspect-ratio microstructures on planar and nonplanar surfaces using a modified LIGA process. *J. Microelectromech. Syst.* **1997**, *6*, 329–336.

17 Zhao, X. M.; Xia, Y. N.; Qin, D.; Whitesides, G. M. Fabrication of polymeric microstructures with high aspect ratios using shrinkable polystyrene films. *Adv. Mater.* **1997**, *9*, 251–254.

18 Kim, K.; Park, S.; Lee, J.-B.; Manohara, H.; Desta, Y.; Murphy, M.; Ahn, C. H. Rapid replication of polymeric and metallic high aspect ratio microstructures using PDMS and LIGA technology. *Microsyst. Technol.* **2002**, *9*, 5–10.

19 Zhou, W. X.; Chan-Park, M. B. Large area UV casting using diverse polyacrylates of microchannels separated by high aspect ratio microwalls. *Lab Chip* **2005**, *5*, 512–518.

20 Zhang, Y.; Lo, C. W.; Taylor, J. A.; Yang, S. Replica molding of high-aspect-ratio polymeric nanopillar arrays with high fidelity. *Langmuir* **2006**, *22*, 8595–8601.

21 Chandra, D.; Yang, S. Capillary-force-induced clustering of micropillar arrays: Is it cause by isolated capillary bridges or by the lateral capillary meniscus interaction force? *Langmuir* **2009**, *25*, 10430–10434.

22 Chandra, D.; Yang, S.; Soshinsky, A. A.; Gambogi, R. J. Biomimetic ultrathin whitening by capillary-force-induced random clustering of hydrogel micropillar arrays. *ACS Appl. Mater. Interfaces* **2009**, *1*, 1698–1704.

23 Hui, C. Y.; Jagota, A.; Lin, Y. Y.; Kramer, E. J. Constraints on microcontact printing imposed by stamp deformation. *Langmuir* **2002**, *18*, 1394–1401.

24 Roca-Cusachs, P.; Rico, F.; Martinez, E.; Toset, J.; Farre, R.; Navajas, D. Stability of microfabricated high aspect ratio structures in poly(dimethylsiloxane). *Langmuir* **2005**, *21*, 5542–5548.

25 Stoykovich, M. P.; Cao, H. B.; Yoshimoto, K.; Ocola, L. E.; Nealey, P. F. Deformation of nanoscopic polymer structures in response to well-defined capillary forces. *Adv. Mater.* **2003**, *15*, 1180–1184.

26 Cohen, A. E.; Mahadevan, L. Kinks, rings, and rackets in filamentous structures. *Proc. Natl. Acad. Sci. U.S.A.* **2003**, *100*, 12141–12146.

27 Bico, J.; Roman, B.; Moulin, L.; Boudaoud, A. Elastocapillary coalescence in wet hair. *Nature* **2004**, *432*, 690.

28 Py, C.; Bastien, R.; Bico, J.; Roman, B.; Boudaoud, A. 3D aggregation of wet fibers. *Europhys. Lett.* **2007**, *77*, 44005.

29 Denkov, N. D.; Velev, O. D.; Kralchevsky, P. A.; Ivanov, I. B.; Yoshimura, H.; Nagayama, K. Mechanism of formation of two-dimensional crystals from latex particles on substrates. *Langmuir* **1992**, *8*, 3183–3190.

30 Chakrapani, N.; Wei, B.; Carrillo, A.; Ajayan, P. M.; Kane, R. S. Capillarity-driven assembly of two-dimensional cellular carbon nanotube foams. *Proc. Natl. Acad. Sci. U.S.A.* **2004**, *101*, 4009–4012.

31 Lee, T. W.; Mitrofanov, O.; Hsu, J. W. R. Pattern-transfer fidelity in soft lithography: The role of pattern density and aspect ratio. *Adv. Funct. Mater.* **2005**, *15*, 1683–1688.

32 Segawa, H.; Yamaguchi, S.; Yamazaki, Y.; Yano, T.; Shibata, S.; Misawa, H. Top-gathering pillar array of hybrid organic-inorganic material by means of self-organization. *Appl. Phys. A: Mater. Sci. Process.* **2006**, *83*, 447–451.

33 Zhao, Y. P.; Fan, J. G. Clusters of bundled nanorods in nanocarpet effect. *Appl. Phys. Lett.* **2006**, *88*, 103123.

34 de Gennes, P. G.; Brochard-Wayrt, F.; Quere, D. *Capillarity and Wetting Phenomena*; Springer: New York, 2004.

35 Kralchevsky, P. A.; Nagayama, K. *Particles at Fluids Interfaces and Membranes*; Elsevier Science: Amsterdam, 2001.

36 Kralchevsky, P. A.; Paunov, V. N.; Ivanov, I. B.; Nagayama, K. Capillary meniscus interaction between colloidal particles attached to a liquid-fluid interface. *J. Colloid Interface Sci.* **1992**, *151*, 79–94.

37 Tanaka, T.; Morigami, M.; Atoda, N. Mechanism of resist pattern collapse during development process. *Jpn. J. Appl. Phys.* **1993**, *32*, 6059–6064.

38 Bernardino, N. R.; Dietrich, S. Comment on biomimetic ultrathin whitening by capillary-force-induced random clustering of hydrogel micropillar arrays. *ACS Appl. Mater. Interfaces* **2010**, *2*, 603–604.

39 Chandra, D.; Yang, S. Response to comment on biomimetic ultrathin whitening by capillary-force-induced random clustering of hydrogel micropillar arrays. *ACS Appl. Mater. Interfaces* **2010**, *2*, 605.

40 Vukusic, P.; Hallam, B.; Noyes, J. Brilliant whiteness in ultrathin beetle scales. *Science* **2007**, *315*, 348.